Protein-induced photophysical changes to the amyloid indicator dye thioflavin T

Leslie S. Wolfe[1], Matthew F. Calabrese[1], Abhinav Nath[1], Dorottya V. Blaho, Andrew D. Miranker[2], and Yong Xiong[2]

Department of Molecular Biophysics and Biochemistry, Yale University, 260 Whitney Avenue, New Haven, CT 06520-8114

Edited by José N. Onuchic, University of California San Diego, La Jolla, CA, and approved August 4, 2010 (received for review March 8, 2010)

The small molecule thioflavin T (ThT) is a defining probe for the identification and mechanistic study of amyloid fiber formation. As such, ThT is fundamental to investigations of serious diseases such as Alzheimer's disease, Parkinson disease, and type II diabetes. For each disease, a different protein undergoes conformational conversion to a β-sheet rich fiber. The fluorescence of ThT exhibits an increase in quantum yield upon binding these fibers. Despite its widespread use, the structural basis for binding specificity and for the changes to the photophysical properties of ThT remain poorly understood. Here, we report the co-crystal structures of ThT with two alternative states of β-2 microglobulin (β2m); one monomeric, the other an amyloid-like oligomer. In the latter, the dye intercalates between β-sheets orthogonal to the β-strands. Importantly, the fluorophore is bound in such a manner that a photophysically relevant torsion is limited to a range of angles generally associated with low, not high, quantum yield. Quantum mechanical assessment of the fluorophore shows the electronic distribution to be strongly stabilized by aromatic interactions with the protein. Monomeric β2m gives little increase in ThT fluorescence despite showing three fluorophores, at two binding sites, in configurations generally associated with high quantum yield. Our efforts fundamentally extend existing understanding about the origins of amyloid-induced photophysical changes. Specifically, the β-sheet interface that characterizes amyloid acts both sterically and electronically to stabilize the fluorophore's ground state electronic distribution. By preventing the fluorophore from adopting its preferred excited state configuration, nonradiative relaxation pathways are minimized and quantum yield is increased.

Alzheimer's | beta-2 microglobulin | Parkinson | TICT | photophysics

The conversion of a normally soluble protein into fibrillar aggregates is of central importance to a range of diseases including Alzheimer's disease, Parkinson disease, and type II diabetes (1). Despite the involvement of distinct proteins in each of these conditions, the fibers formed share a common set of structural and biophysical properties, which define them as amyloid. Amyloid fibers are homopolymeric, noncovalent assemblies, which present morphologically as twisted sets of unbranched filaments. These filaments are composed of two or more β-sheets whose strands run in a direction orthogonal to the long axis of the fiber (2, 3). This arrangement yields a characteristic cross-β pattern by X-ray diffraction, the presence of which represents the gold standard for unequivocal identification of amyloid structure (4, 5).

As the routine use of diffraction has proven impractical for most mechanistic studies of amyloid assembly, a considerable fraction of the publication record relies in whole or in part on the use of benzothiazole dyes, most commonly thioflavin T (ThT) (Fig. 1*A*). The breadth of their use includes histological, kinetic, imaging, and structural studies (6, 7). ThT was first reported as a tool for detecting amyloid in ex vivo tissue samples in 1959, and this interaction was suggested to be highly specific for amyloid-like structures (8). In later years, ThT was characterized biophysically, resulting in its broad acceptance as a defining characteristic for the presence of amyloid (9). The changes in the fluorescent properties of ThT upon binding amyloid include a shift in its excitation spectrum and an increase in quantum yield (Fig. 1*D*, *Inset*, and Fig. S1) (9). ThT in protic solvents principally absorbs at 340 nm with an emission maximum at 445 nm. Upon binding amyloid-like states, a peak at approximately 440 nm becomes dominant with the fluorescent emission maximum shifted to 480 nm. This is accompanied by a strong enhancement of the fluorescence. These changes are collectively referred to as a "ThT positive" state. Despite the extensive use of ThT as an indicator dye, the structural basis of its interactions with amyloid and amyloid-like states remains poorly understood (10).

Recently, we reported the crystal structure of an amyloid-like oligomer of β-2 microglobulin (β2m) (11). β2m is the 12 kDa light chain noncovalently associated with the Class I Major Histocompatibility complex (MHC) (12). It directs proper folding and cell-surface expression of MHC. As part of normal cellular turnover, β2m is released to the serum and catabolized by the kidneys. In patients on long-term hemodialysis therapy, serum levels are elevated and β2m deposits as amyloid plaques. This conversion can be induced in vitro by exposure to Cu^{2+}. Under such conditions, β2m self-associates to populate closed amyloid-like oligomers prior to mature fiber formation (13). These nonfibrillar, amyloid-like states are ThT positive in solution yet are amenable to crystallization, providing a unique opportunity for structural analysis (11, 13). In this work, we determine the crystal structures of ThT bound to both amyloid-like and nonamyloid states of β2m. These structures allow for an interrogation of the structural basis of ThT fluorescence enhancements as well as a direct comparison of the structures of ThT positive and negative states.

Results

In order to investigate the structural basis of ThT–amyloid interactions, we first prepared two sets of β2m crystals in the presence ($\beta 2m_{holo}$) and absence ($\beta 2m_{apo}$) of its metal ligand, Cu^{2+}. $\beta 2m_{apo}$ is monomeric and well behaved under physiological solution conditions. In contrast, the *holo* state undergoes conformational changes resulting in the formation of a hexameric species (11, 13). Long-term incubation at 37 °C results in aggregation of $\beta 2m_{holo}$ but not $\beta 2m_{apo}$ (14). Both sets of crystals were prepared in the presence of 5 mM ThT. We then directly analyzed the fluorescence properties of the crystals. This was followed by a determination of the structures of these two states at atomic resolution.

Co-crystals of ThT : $\beta 2m_{holo}$ show strong fluorescence intensity when compared to ThT : $\beta 2m_{apo}$. Crystals were imaged using both near-UV (340 nm) and blue (440 nm) excitation light to enable

Author contributions: L.S.W., M.F.C., A.N., and A.D.M. designed research; L.S.W., M.F.C., A.N., D.V.B., A.D.M., and Y.X. performed research; L.S.W., A.N., A.D.M., and Y.X. analyzed data; and L.S.W. and A.D.M. wrote the paper.

The authors declare no conflict of interest.

This article is a PNAS Direct Submission.

Data deposition: The atomic coordinates have been deposited in the Protein Databank, www.pdb.org (PDB ID codes 3MYZ and 3MZT).

[1]L.S.W., M.F.C., and A.N. contributed equally to this work.

[2]To whom correspondence may be addressed. E-mail: andrew.miranker@yale.edu or yong.xiong@yale.edu.

This article contains supporting information online at www.pnas.org/lookup/suppl/doi:10.1073/pnas.1002867107/-/DCSupplemental.

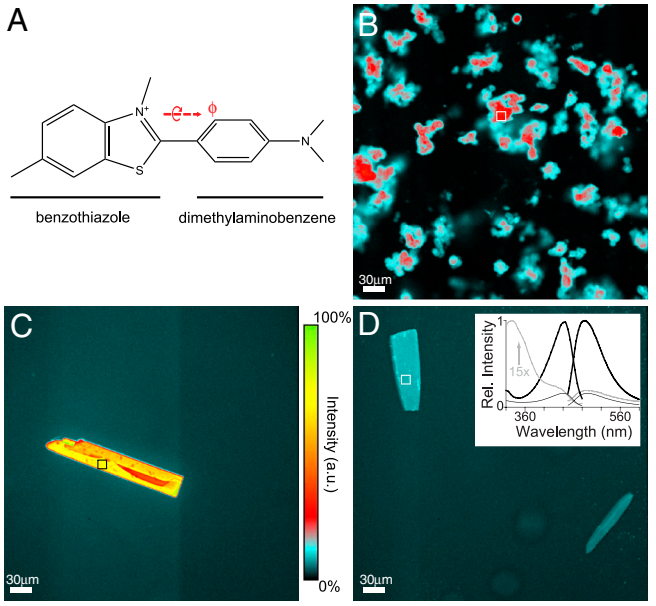

Fig. 1. Visualization of ThT in protein crystals and aggregates. (*A*) The chemical structure of ThT. The angle ϕ is defined by the torsion angle between the benzothiazole ring and the dimethylaminobenzene ring (20). $\phi = 0$ corresponds to coplanarity of the two aromatic moieties. (*B–D*) False-color fluorescence images collected using blue-light (440 nm) excitation of human islet amyloid fibers, $\beta 2m_{holo}$ crystals and $\beta 2m_{apo}$ crystals respectively. Relative intensity across panels *B* and *D* are directly comparable and use the same indicated color scale. Ratiometric measures quoted in the main text use signal integrated across the areas indicated with a box. Ratios were computed using the same areas on images collected using 340 nm excitation (see also Fig. S2). (*Inset*) Fluorescence excitation (Em_{492}) and emission spectra (Ex_{440}) for 100 μM β2m, 100 μM ThT, 200 mM potassium acetate and 25 mM MOPS at pH 7.4 and 25 °C. Samples contained either 200 μM Cu^{2+} (black) or 10 mM EDTA (gray). The latter is shown on the same relative scale as the former. The excitation spectrum of the latter is further shown scaled by a factor of 15.

ratiometric measurements of fluorescence. Co-crystals of ThT : $\beta 2m_{holo}$ show approximately 28-fold more intensity when excited at 440 nm than at 340 nm (Fig. 1*C* and Fig. S2*A*). In contrast, crystals of ThT : $\beta 2m_{apo}$ displayed a more modest, approximately eightfold increase in relative intensity (Fig. 1*D*). The magnitude of fluorescence enhancement can be compared to amyloid fibers prepared from human islet amyloid polypeptide (15). These show a ratiometric increase in intensity of approximately 15 (Fig. 1*B*). Negative control samples, including cross-linked aggregates of bovine serum albumin, generated ratiometric enhancements between 5 and 6, which was comparable to background (Fig. S2). To eliminate the possibility of subjectivity, several sets of crystals and their images were collected in a single-blind format, with the identity of the crystals concealed from the experimenter. In these cases, ThT : $\beta 2m_{holo}$ could be readily distinguished from ThT : $\beta 2m_{apo}$ on the basis of its total intensity when illuminated at 440 nm. Thus, ThT responds to $\beta 2m_{holo}$ in crystals in a manner that parallels what is observed for amyloid fibers. Furthermore, both $\beta 2m_{holo}$ and $\beta 2m_{apo}$ qualitatively parallel the published behavior of ThT:β2m interactions as monitored in dilute solution (Fig. 1*D*, *Inset*, and Fig. S1) (13).

ThT is bound at an oligomeric, intersheet interface of two $\beta 2m_{holo}$ molecules. The crystal structure of $\beta 2m_{holo}$ consists of six monomers arranged in a ring. Three symmetric occurrences of each of two distinct interfaces mediate hexamer formation. ThT molecules reside at an intersheet interface formed by two, four-stranded β-sheets (Fig. 2*A*) with the orientation of the long axis of ThT at a right angle to the β-strands (Fig. 3*B*). Superposition of one chain (chain D) from the ligand bound structure solved here with the same chain from our deposited $\beta 2m_{holo}$ structure (11) (chain D) gives an rmsd of 0.39 Å for the C_α positions (Fig. 2*B*, *Left*). Thus, only modest deviations occur at the main chain. Most alterations are apparent at side chains within the interface, notably Gln8, Tyr10, and Tyr26. The maximum change appears limited to a rotamer change in Tyr10, which results in a 2 Å shift in the position of the side-chain hydroxyl group (Fig. 2*B*, *Left*). If instead, alignment is performed using one of the pairs of chains that form the ThT binding pocket (chains D and E), a C_α rmsd of 0.69 Å is observed. In effect, chain E has moved approximately 1.5 Å away from chain D in comparison to our previously published structure (11) (Fig. 2*B*, *Right*). The change in the respective C_α positions reflects a simple increase in overall separation of the two subunits from one another in order to accommodate the fluorophore. We additionally note that the binding site is symmetric at this location. Indeed, two equivalent alternative conformations of ThT can be modeled at this site with the benzothiazole ring stacking in parallel with one or the other of the Tyr10 residues (Fig. 3*A* and Figs. S3 and S4*A*). For both conformations, it is clear that ThT is buried within a β-sheet interface whose structure requires only modest alteration to accommodate the fluorophore.

In $\beta 2m_{holo}$, the binding pocket of the benzothiazole ring is well defined and dominated by the side chains of Tyr10 and Tyr26. Contacts made by the benzothiazole ring include aromatic stacking with Tyr10 in a configuration that includes cation–π and π–π interactions (Fig. 3*C*). While density for the benzothiazole ring is well defined, density for the dimethylaminobenzene portion of the fluorophore appears limited to a rotationally averaged contribution along the ϕ-axis (Fig. 3*A* and Fig. S4*A*). However, the fixed position of the benzothiazole ring necessarily restricts the location and orientations available to the dimethylaminobenzene ring. Rotation about the angle ϕ is the only available degree of freedom. Importantly, residues Gln8 from each of the protein chains have clearly defined density (Fig. 3*B*), and these limit the range of angles available to this rotation. The dimethylaminobenzene ring can be modeled with ϕ values between 57° and 102°. Rotations greater than 102°, or less than 57°, result in steric clashes with the Gln8 side chains of the binding pocket (Fig. 3*B*). Thus, we reason that the dimethylaminobenzene ring samples a disordered but narrow range of configurations as a consequence of bounded rotations about the carbon–carbon bond that defines the ϕ-axis.

The structure of $\beta 2m_{apo}$ supports two distinct binding sites for ThT. Two copies of β2m, differing from each other by a C_α rmsd of 1.2 Å, are present in the asymmetric unit of $\beta 2m_{apo}$ (Fig. 4). Within these co-crystals, the β2m molecules have adopted a configuration closely associated with other known *apo* forms of the protein. Most notably, the $\beta 2m_{apo}$ shows Pro32 to be in a *cis*-conformation, while in $\beta 2m_{holo}$ it is *trans*-. In addition, Phe30 is a completely buried residue in $\beta 2m_{apo}$, while it is fully exposed in $\beta 2m_{holo}$. These differences are compatible with previous analyses (11, 16, 17). One of the binding sites for ThT accommodates two fluorophores, which bind at a slight angle in relation to the backbone of the β-strands and reside at an interface between the two protein molecules in the asymmetric unit of the crystal (Fig. 4*A*). The second site resides at a crystallographic interface formed from three molecules of β2m (Fig. 4*B–C*). In total, the ratio of ThT to protein in the *apo* state is 3:2.

ThT stacks as an antiparallel dimer in the first binding site formed by $\beta 2m_{apo}$. The residues that define the position of the ThT dimer are the same as those seen in $\beta 2m_{holo}$, namely Tyr10, Tyr26, and Gln8 (rendering of Gln8 omitted in Fig. 4*A* for clarity). However, the orientation of the fluorophores relative to the β-sheet is not orthogonal. Instead, the ThT molecules cross the β-sheets of β2m at an approximately 25° angle. In addition, the dimethylaminobenzene ring is nearly parallel to the benzothiazole ring ($\phi = 29$) unlike the nearly orthogonal orientation adopted when binding to $\beta 2m_{holo}$. We further observe that the position

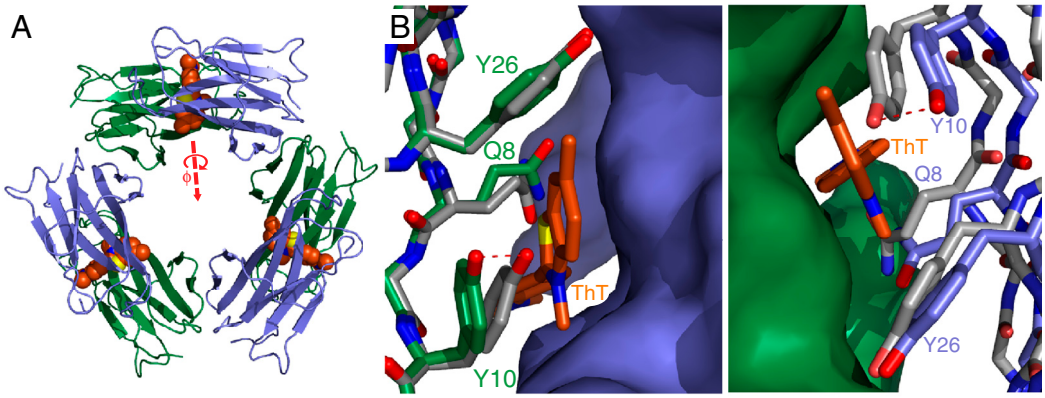

Fig. 2. ThT at the subunit interfaces of $\beta 2m_{holo}$. (*A*) A ribbon representation of the $\beta 2m_{holo}$ hexamer. This is a trimer of dimers with alternate subunits drawn in blue and green. The ThT molecules are drawn in orange and can be seen intercalated at right angles to the strands of the intersheet interfaces. (*B*) Close up of a single, two-subunit interface with either one (*Right*) or the other (*Left*) of the subunits drawn as a surface while the other is shown as sticks. Two subunits from the ThT-free crystal structure of this hexamer are shown as white sticks (PDB ID: 3CIQ). Note, alignment of the two subunits was deliberately performed using only backbone atoms of the left (green) subunit. This results in the left panel showing only side-chain rotamer changes while the right panel captures all of the subunit–subunit displacements.

of both rings of both ThT molecules are well defined. This is evident in the fact that density is resolved for the whole of the fluorophores (Fig. S4*B*). Dimerization of ThT is an observation consistent with its amphiphilic nature. Amphiphile induced colloidal interactions have previously been reported as a possible origin for amyloid association (18). Such structures can be expected to form from amphiphiles, and, indeed, the stacking conformation we directly observe here is one of four ways it has been suggested that two molecules of ThT might self-associate (19).

The second ThT binding site occurs at a crystallographic interface and makes contact with three symmetry-related β2m monomers (Fig. 4 *B*–*C*). The dimethylaminobenzene ring of this ThT stacks with Trp60 of one β2m monomer, while the benzothiazole ring is sandwiched between the side chains of two different β2m monomers. Notable contacts include Asn42 and Arg81 (Fig. 4*B*). This binding site is also well defined and yields a ThT internal geometry of $\phi = \sim 30°$.

Discussion

In this work, we report the atomic structures of ThT bound to crystals of amyloid-like $\beta 2m_{holo}$ and nonamyloid $\beta 2m_{apo}$. Our results clearly indicate that (*i*) there is an increase in the quantum yield of ThT measured directly in $\beta 2m_{holo}$ crystals, while $\beta 2m_{apo}$ crystals only show modest enhancement; (*ii*) ThT:protein interactions are stabilized in both β2m forms by stacking with aromatic amino acids; (*iii*) the two conjugated rings of ThT sample a disordered, albeit limited range of relative orientations in $\beta 2m_{holo}$. The same torsion angle in $\beta 2m_{apo}$ is fixed; (*iv*) ThT binds to $\beta 2m_{holo}$ in a direction orthogonal to the β-strands of the protein, while this is not observed in $\beta 2m_{apo}$. These key observations offer a comprehensive description of how ThT binds to macromolecules and how such interactions with amyloid states can give rise to its characteristic photophysical changes.

The observed structure of ThT in $\beta 2m_{holo}$ is not compatible with existing descriptions of the origins of amyloid-induced increases in ThT quantum yield. The fluorescence of thioflavin T is strongly influenced by its conformational and electronic properties. The rings of ThT can be regarded as two rigid planes separated by a single bond about which rotation can occur (ϕ). The gas-phase minimum energy conformation of ThT is not coplanar ($\phi = 0°$). Rather, the N-methyl group of the benzothiazole ring gives a steric clash resulting in an optimal angle of $\phi = 37°$ (20). Upon absorption of a photon, ThT enters an electronic excited state. The calculated gas-phase minimum energy conformation in this excited state is $\phi = 90°$ (Fig. 5*A*). Within the con-

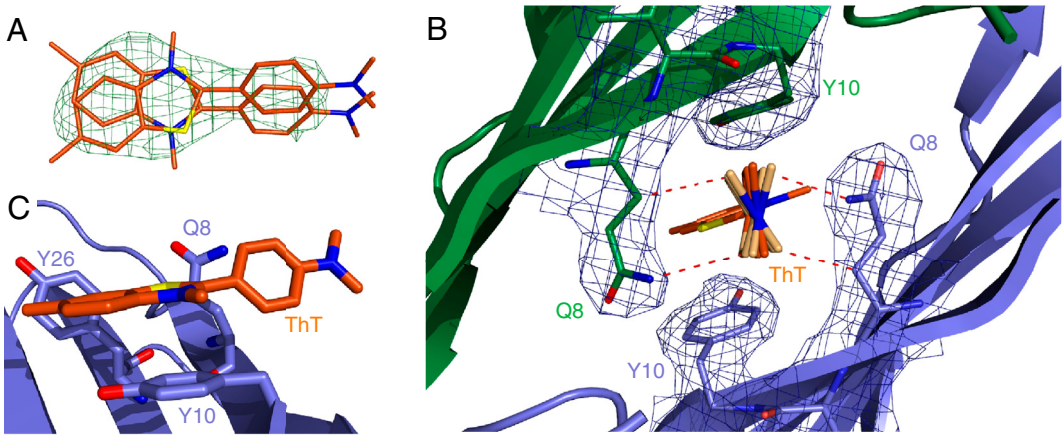

Fig. 3. Experimental, steric, and electronic constraints affecting interactions of ThT with $\beta 2m_{holo}$. (*A*) $F_o - F_c$ electron difference density for ThT bound to $\beta 2m_{holo}$ contoured at 3σ. The binding pocket allows for two, symmetry-related orientations of the fluorophore. Density around the benzothiazole ring is clearly observed. Density for portions of the benzene ring approximately colinear with ϕ is also apparent while the dimethylamino group appears wholly disordered. (*B*) Electron density for Gln8 and Tyr10 of the ThT binding pocket contoured at 1σ. The dimethylaminobenzene ring of ThT can adopt a range of ϕ angles in this pocket (see main text). The two most divergent possibilities are drawn as superpositions in light orange. (*C*) The nitrogen of the benzothiazole ring is located 3.8 Å over the center of the phenol ring of Tyr10 suggesting stabilization by cation-π interactions.

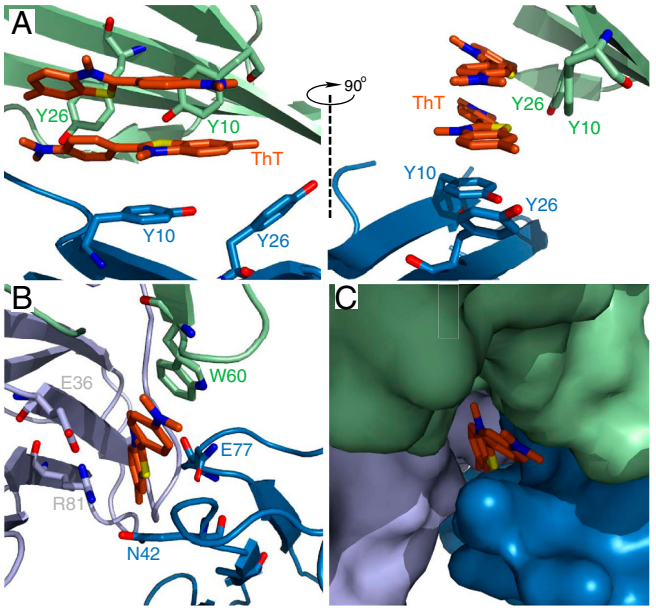

Fig. 4. Molecular structure of the two ThT binding sites in $\beta 2m_{apo}$. $\beta 2m_{apo}$ is monomeric in solution. Associations with ThT are apparent at crystallographic interfaces. Subunits are drawn in green, blue and gray, respectively. (*A*) This binding site accommodates two molecules of ThT bound in an antiparallel orientation. Two panels are shown related by the indicated 90° rotation. (*B* and *C*) The second binding site is formed by three subunits of $\beta 2m_{apo}$. These are shown with ribbons and sticks in *B* and as surfaces in *C*.

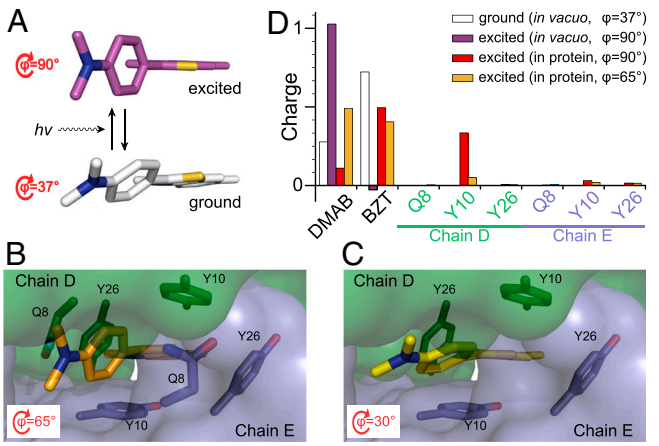

Fig. 5. Geometry-optimized structures and charge distributions of ThT calculated using ab initio methods. (*A*) The gas-phase ground state energetic minimum of ThT (white) is located at $\phi = 37°$. In nonviscous solvents, absorption of a photon is followed by relaxation to the excited state energetic minimum at $\phi \sim 90°$ (magenta). This corresponds to a nonfluorescent state (see main text). (*B*) In the presence of the binding pocket, the energetic minimum of ThT in the excited state is at $\phi = 65°$. Protein subunits are shown as solvent accessible surfaces in blue and green. Six protein side chains comprise the binding site (Gln8, Tyr10, and Tyr26 from each of two chains, shown as sticks). Only these residues and ThT are included in the calculations; hydrogen atoms are omitted from *A*–*C* for clarity. (*C*) Removal of Gln8 from the calculations leaves only a four-residue tyrosine cage. Here, ThT converges to $\phi = 30°$ in the excited state. (*D*) Calculated charge distributions for ThT and binding site residues. For each calculation, charges were summed across the indicated side chain and the dimethylaminobenzene (DMAB) and benzothiazole (BZT) moieties of ThT. These sums are shown as histogram bars. Colors of ThT in panels *A*–*C* are maintained in the histogram as appropriate.

formational ensemble of the excited state, the charge on the benzothiazole ring can either remain localized or delocalize over the combined ring system. The latter is calculated to occur for ϕ angles $> \sim 60°$. This phenomenon, known as twisted intramolecular charge transfer (TICT), is relevant because the quantum yield of ThT in this state approaches zero (20). Thus, ThT is only weakly fluorescent in free solution because after it absorbs a photon it proceeds to a state with a ϕ angle >60°. If conditions are such that rotation about ϕ is restricted by protein binding, or by solvent viscosity, then the time required to rotate to $\phi > 60°$ is greater than the lifetime of the excited state, and radiative decay occurs. Such fluorescence from conformations with $\phi < \sim 60°$ is said to occur from a locally excited (LE) state. This is the generally accepted basis for the enhancement of ThT fluorescence for amyloids (7, 21–24). Intriguingly, the crystal structure of $\beta 2m_{holo}$ with ThT is wholly at odds with this characterization because density for the dimethylaminobenzene ring is suggestive of a disordered range of ϕ angles, all of which are >60°.

Aromatic interactions may be the origin for the observed increase in fluorescence of ThT bound to $\beta 2m_{holo}$ crystals. In order to reconcile the observed increase in quantum yield of ThT with its apparent access to only nonradiative TICT states near $\phi = 90°$, we pursued quantum chemistry calculations. Gas-phase computation of ThTwas compared to ThT in the presence of the $\beta 2m_{holo}$ binding pocket. The latter was represented by the four side chains that comprise an aromatic cage (i.e., two each of Tyr10 and Tyr26) and the two Gln8 side chains that limit ϕ to between 102° and 57°. In agreement with previous reports (25), we observe the minimum configuration of the first excited state in the gas phase to be at $\phi = 90°$ (Fig. 5*A*). The presence of the binding pocket causes the excited state of ThT to instead converge to a configuration at $\phi = 65°$ (Fig. 5*B*). Most remarkably, we observe that upon removing the Gln8 side chains from the calculation, ab initio excited state minimization results in a shift to $\phi = 30°$ (Fig. 5*C*). Plainly, rotation of the dimethylaminobenzene group away from the in vacuo optimum at $\phi = 90°$ is strongly driven by the aromatic interactions with the benzothiazole moiety and has minimal influence from contacts with Gln8. Thus, binding at the $\beta 2m_{holo}$ interface has dramatically changed the conformational landscape of the excited state of ThT to one in which more planar, fluorescent conformations are stabilized. We note the general observation that aromatic residues are strong contributors to the amyloidogenicity of peptide sequences (26). The enhanced propensity of amyloid formation by aromatic residues may therefore also yield interfaces that readily bind and stabilize the electronic distribution of ThT.

Charge stabilization may account for the increased quantum yield for ThT in $\beta 2m_{holo}$ despite being bound with relatively unrestricted access to what are nominally TICT dark states at $\phi > 60°$. In gas-phase calculations of the ground state at $\phi = 37°$, about $+0.3e$ of the $+1e$ overall charge on ThT is localized to the dimethylaminobenzene group (Fig. 5*D*). The calculated gas-phase charge distribution for ThT held at $\phi = 90°$ is significantly shifted such that the dimethylaminobenzene moiety bears slightly over $+1e$ while the benzothiazole group displays a slight negative charge. This coupling of charge transfer to rotational conformation is a well known characteristic of a class of fluorophores that includes ThT (25, 27). ThTcan be held in its gas-phase optimum of $\phi = 90°$ in the presence of the binding site without causing steric clash (Fig. 5*D*). Remarkably, the intramolecular charge transfer apparent in vacuo is dramatically reversed: The charge on the dimethylaminobenzene ring decreases from $+1.03e$ to $+0.11e$. Direct involvement of the tyrosine residues is evident in these calculations by the fact that charge delocalization includes redistribution of $+0.33e$ to one of the coplanar side chains of Tyr10. Protein-mediated charge stabilization continues to affect the electronic distribution of ThT at $\phi = 65°$: charge on the dimethylaminobenzene ring decreases from $+0.74e$ in vacuo to $+0.49e$ in the presence of the protein. In other words, the $\beta 2m_{holo}$ binding site alters the charge distribution of ThT at $\phi = 65°$ so that it more closely approaches that calculated for

the fluorescent LE state at $\phi \sim 25°$. The importance of these changes in electronic distribution to fluorescent behavior is further illustrated by calculations of oscillator strength, a dimensionless quantity that reflects the strength of a radiative electronic transition. The oscillator strength of ThT increases from 0.0007 in vacuo to 0.14 in the presence of the protein at $\phi = 90°$. A further increase to 0.74 is calculated for ThT in the presence of the protein at $\phi = 65°$. These measures are in excellent agreement with the observation that the TICT state of ThT is radiatively silent while $\beta 2m_{holo}$-bound ThT is brightly fluorescent. Thus, protein-mediated stabilization of charge to the benzothiazole ring of ThT is the likely primary mechanism of fluorescence enhancement.

Stabilization of charge may be a general contributor to amyloid-like induced changes to ThT fluorescence. For example, outer surface protein A (OspA) from *Borrelia* has recently been engineered to make cross β-like interactions in a soluble domain (7, 23). This is made possible by the presence of a surface-exposed antiparallel β-sheet composed of eight strands. ThT gives an increase in fluorescence intensity in the presence of OspA variants, provided the variants include a collinear stack of at least four tyrosine residues (7, 24). Despite reported attempts and the observation that crystal quality is improved by the inclusion of ThT, electron density could not be observed for the fluorophore. We surmise that ThT is bound in OspA in a manner similar to what we directly observe here in $\beta 2m_{holo}$, i.e., the dimethylaminobenzene ring of ThT is disordered when bound to OspA and that its charge localization is stabilized by aromatic and cation–π interactions in the binding pocket. Visible wavelength CD of these complexes are also reported to have marked negative ellipticity at approximately 420 nm. This is calculated to derive from a twisted conformation about ϕ (28). This observation has been reported for amyloid fibers formed from insulin (29) as well as the fungal prion protein HET-s (30). To be clear, rotational mobility is not essential to this mechanism. Rather protein binding can stabilize conformations of ThT where ϕ may be greater than 60°. Such binding events must also include contacts that stabilize charge in order to minimize TICT relaxation pathways.

$\beta 2m_{apo}$: ThT co-crystals show a modest increase in fluorescence intensity that is consistent with a rigid fluorophore environment being the origin of enhanced quantum yield. The three ThT molecules in the two sites all show well defined density resulting in ϕ-angles of 29°. This is close to the calculated low energy conformation (20). Furthermore, the B-factors for these ThT molecules are closely similar to those of the core backbone atoms of the protein. These observations strongly suggest a rigid environment. This can be compared to observations that show increased quantum yield for ThT in viscous solvents such as glycerol (21). Greatly enhanced fluorescence is also seen in the only other crystal structure of protein-bound ThT. The protein acetylcholinesterase from electric eel binds ThT in a nonamyloid binding pocket that also renders the fluorophore rigid (22). These authors modeled the two-ring system as coplanar, although modest angles $< \sim 20°$ also appear compatible with the deposited structure factors. A total of five aromatic groups form the binding pocket. Thus, stabilization of ThT near its ground state conformation is sufficient for fluorescence enhancement. For the $\beta 2m_{apo}$: ThT complex, one of the two ThT sites contains two ThT molecules stacked colinearly. This binding mode is suggestive of either the presence of an excimer (31) or alternatively results in autoquenching. We do not observe significant red shifts in emission wavelength that might be attributed to the formation of an excimer (Fig. S1). We note that a single cation–π interaction between one of the Tyr10 residues and one of the ThT molecules in the stack is present (Fig. 4*A*). Given the absence of fluorescence intensity enhancement (Fig. 1*D*), it is most likely that this pair of ThT molecules in the $\beta 2m_{apo}$ structure is quenched.

The use of ThT is widespread in structural and mechanistic studies of amyloid formation. Changes in its intensity are used not only as a qualitative indicator of amyloid but also as a quantitative measure of amyloid formation. Extents of conversion are used, for example, in assessing mutational or small molecule inhibition effects. Here we have shown that the key features of ThT binding to an amyloid-like state include monomeric intercalation within β-sheets at an angle orthogonal to the β-sheet axis as well as stabilization of the fluorophores's electronic distribution. The former is consistent with changes observed in diffraction of insulin fibers in the presence and absence of ThT (19) as well as assessment of ThT polarization from mechanically oriented insulin fibers (32). Electronic stabilization can result from structural rigidity. We find that rigidity such as that observed in $\beta 2m_{apo}$ is sufficient, but not necessary, for ThT fluorescent enhancement. Instead, we have observed direct interactions of the charge on ThT with the $\beta 2m_{holo}$ binding pocket. The quantum yield of ThT is well known to be variable among different proteins. Here, we have shown that this variability derives from a rich structural complexity that can include steric hindrance, electronic stabilization, and autoquenching. Our hope is that this and subsequent insights will lead to a depth of understanding that permits fluorescence enhancement of ThT by amyloids to be delineated from amyloid-like and from nonamyloid (false-positive) binding modes. Moreover, rational design of ThT derivatives may allow greater selectivity and/or sensitivity to amyloid states. Such approaches will enable ThT to move beyond its role of simply serving as a qualitative indicator of amyloid formation. Instead, ThT and its descendents can hope to report on the specifics of local structural and motional properties of this important protein state.

Materials and Methods

Materials. Buffers, salts, and ThT were obtained from Sigma, Aldrich, J. T. Baker, American Bioanalytical and Acros. Cloning and expression cell lines were obtained from Stratagene and Novagen. Islet amyloid polypeptide was synthesized by standard t-Boc methods and purified by the W.M. Keck facility (New Haven, CT). Lipids for Nanodiscs were acquired from Avanti Polar Lipids and scaffold protein MSP1D1 was kindly provided by Stephen G. Sligar (University of Illinois, Urbana-Champaign).

Crystallization. Crystals of the H13F construct of $\beta 2m_{holo}$ and $\beta 2m_{apo}$ were obtained by sitting-drop vapor diffusion as previously described (11) except for the addition of 5mM ThT. Crystals were frozen in liquid propane with 5 mM ThT, 20% glycerol, 50 mM diammonium tartrate and 22.5% PEG 3350. Diffraction data were collected at the NECAT beamline ID24 at the Advanced Photon Source (Argonne, IL) and the Brookhaven National Lab beamlines X29 and X25 (Upton, NY).

Structure Determination. The $\beta 2m_{holo}$ crystals belong to space group $P2_12_12$ and diffracted to 2.7 Å resolution. The structure was determined by molecular replacement using the coordinates from a hexamer β2m structure (PDB ID: 3CIQ) (11). The program Phaser (33) was used for the molecular replacement. The asymmetric unit contains six β2m molecules arranged in a hexamer as a trimer of dimers. After rigid body and restrained refinement in Refmac5 (34), and rebuilding using Coot (35), the density for ThT was clearly visible in the $F_o - F_c$ difference electron density map before its inclusion in the model (Fig. S4). The electron density was further improved by sixfold averaging using DM (36). ThT was then fit into the density map and iterative cycles of model building and refinement were carried out using Refmac5 and Phenix (34, 37). The intrinsic symmetry of the hexamer gives rise to alternative, equivalent conformations of ThT binding at each dimer interface, which were built and refined with 50% occupancy each (Fig. S3). The final model has an R/R-free factor of 23.9/25.6%. The data and refinement statistics are summarized in Table S1. Coordinates have been deposited with the PDB accession code 3MZT.

The $\beta 2m_{apo}$ crystals belong to space group $P2_1$ and diffracted to 1.6 Å resolution. The structure was solved by molecular replacement using coordinates from a monomer β2m structure (PDB ID 1KPR) (16). The asymmetric unit contains two copies of β2m. Refinement and rebuilding of $\beta 2m_{apo}$ was similar to that of $\beta 2m_{holo}$ described above, which were performed until the ThT density was clearly visible in the $F_o - F_c$ difference electron density map before its inclusion in the model (Fig. S4). This structure reveals the pre-

sence of two binding sites for ThT, which accommodate a total of three molecules of ThT. The final model has an R/R-free factor of 18.6/22.1%. The data and refinement statistics are summarized in Table S1.

Imaging. Crystals were imaged using an IX71 inverted microscope (Olympus, Center Valley, PA) coupled to an X-Cite 120 lamp (Exfo, Mississauga, ON). Crystals were illuminated through either a 340/10 (near-UV) excitation filter (Thorlabs, Newton, NJ) or a 440/20 (blue) excitation filter (Chroma, Brattleboro, VT), and fluorescence was collected through a 490/40 emission filter (Chroma) using an iXon EMCCD camera (Andor, South Windsor, CT). All images were collected with identical lamp power, gain, and exposure settings for a given excitation filter, enabling quantitative comparisons of ThT intensity. To circumvent low signal-to-noise in the near-UV images (a function of instrumental lamp power and detector efficiency at the wavelengths involved), we obtained ratiometric estimates of ThT fluorescence enhancement for each sample by integrating fluorescence from the same 16 x 16-pixel area under separate blue and near-UV excitation and dividing the former by the latter.

Computational Methods. Ground state geometries and energies were calculated by ab initio RHF (restricted Hartree-Fock) methods implemented in the GAMESS (US) package (38) using the 3-21G basis set. Excited state geometries and energies were calculated using the configuration interaction with singles (CIS) method, also using the 3-21G basis set. The CIS/3-21G/RHF method represents a good compromise between rigor and computational cost for the geometry optimization of large systems such as ThT within the $\beta 2m_{holo}$ binding site.

The geometry of ThT in the first excited state was optimized in the gas phase to generate the $\phi = 90°$ state. This conformation was then aligned with the coordinates of ThT bound at the interface of chains D and E of the $\beta 2m_{holo}$ crystal structure. The system for ab initio calculations consisted of ThT and the side-chain atoms of residues Gln8, Tyr10, and Tyr26 of both protein chains. All six residues were truncated at their β-carbons, which were represented by methyl groups, and hydrogen atoms were added as necessary. Constrained geometry optimization was then performed, wherein all atoms of ThT and hydrogen atoms of the protein were allowed to relax while protein heavy atoms were frozen. Charge distributions based on the Löwdin population analysis (39) and oscillator strengths for states of interest were calculated as implemented in GAMESS.

ACKNOWLEDGMENTS. The authors thank C. A. Schmuttenmaer for helpful discussions, E. Rhoades and M. Rubio for critical reading of the manuscript, J. Hebda for experimental assistance, and synchrotron staff at NE-CAT beamline ID24 and NSLS beamlines X25 and X29 for assistance in data collection. This work was supported, in part, by National Institutes of Health Grant DK54899 (to A.D.M.), an American Heart Association postdoctoral fellowship (A.N.), and National Institutes of Health Institutional Training Grant GM007223 (to L.S.W.)

1. Chiti F, Dobson CM (2006) Protein misfolding, functional amyloid, and human disease. *Annu Rev Biochem* 75:333–366.
2. Tycko R (2006) Molecular structure of amyloid fibrils: Insights from solid-state NMR. *Q Rev Biophys* 39(1):1–55.
3. Bennett MJ, Sawaya MR, Eisenberg D (2006) Deposition diseases and 3D domain swapping. *Structure* 14(5):811–824.
4. Jahn TR, et al. (2010) The common architecture of cross-beta amyloid. *J Mol Biol* 395 (4):717–727.
5. Ferguson N, et al. (2006) General structural motifs of amyloid protofilaments. *Proc Natl Acad Sci USA* 103(44):16248–16253.
6. Groenning M (2009) Binding modeof Thioflavin T and other molecular probes in the context of amyloid fibrils-current status. *J Chem Biol.*
7. Biancalana M, Makabe K, Koide A, Koide S (2009) Molecular mechanism of thioflavin-T binding to the surface of beta-rich peptide self-assemblies. *J Mol Biol* 385(4): 1052–1063.
8. Vassar PS, Culling CF (1959) Fluorescent stains, with special reference to amyloid and connective tissues. *Arch Pathol* 68:487–498.
9. LeVine H, III (1993) Thioflavine T interaction with synthetic Alzheimer's disease beta-amyloid peptides: Detection of amyloid aggregation in solution. *Protein Sci* 2(3):404–410.
10. Biancalana M, Koide S Molecular mechanism of Thioflavin-T binding to amyloid fibrils.. *Biochim Biophys Acta* 1804(7):1405–1412.
11. Calabrese MF, Eakin CM, Wang JM, Miranker AD (2008) A regulatable switch mediates self-association in an immunoglobulin fold. *Nat Struct Mol Biol* 15(9):965–971.
12. Peaper DR, Cresswell P (2008) Regulation of MHC class I assembly and peptide binding. *Annu Rev Cell Dev Biol* 24:343–368.
13. Eakin CM, Attenello FJ, Morgan CJ, Miranker AD (2004) Oligomeric assembly of native-like precursors precedes amyloid formation by beta-2 microglobulin. *Biochemistry* 43(24):7808–7815.
14. Morgan CJ, Gelfand M, Atreya C, Miranker AD (2001) Kidney dialysis-associated amyloidosis: A molecular role for copper in fiber formation. *J Mol Biol* 309(2):339–345.
15. Hebda JA, Miranker AD (2009) The interplay of catalysis and toxicity by amyloid intermediates on lipid bilayers: insights from type II diabetes. *Ann Rev Biophys* 38:125–152.
16. Eakin CM, Berman AJ, Miranker AD (2006) A native to amyloidogenic transition regulated by a backbone trigger. *Nat Struct Mol Biol* 13(3):202–208.
17. Collins EJ, Garboczi DN, Wiley DC (1994) Three-dimensional structure of a peptide extending from one end of a class I MHC binding site. *Nature* 371(6498):626–629.
18. Khurana R, et al. (2005) Mechanism of thioflavin T binding to amyloid fibrils. *J Struct Biol* 151(3):229–238.
19. Groenning M, et al. (2007) Binding modeof Thioflavin T in insulin amyloid fibrils. *J Struct Biol* 159(3):483–497.
20. Stsiapura VI, Maskevich AA, Kuzmitsky VA, Turoverov KK, Kuznetsova IM (2007) Computational study of thioflavin T torsional relaxation in the excited state. *J Phys Chem A* 111(22):4829–4835.
21. Stsiapura VI, et al. (2008) Thioflavin T as a molecular rotor: Fluorescent properties of thioflavin T in solvents with different viscosity. *J Phys Chem B* 112(49):15893–15902.
22. Harel M, Sonoda LK, Silman I, Sussman JL, Rosenberry TL (2008) Crystal structure of thioflavin T bound to the peripheral site of Torpedo californica acetylcholinesterase reveals how thioflavin T acts as a sensitive fluorescent reporter of ligand binding to the acylation site. *J Am Chem Soc* 130(25):7856–7861.
23. Biancalana M, Makabe K, Koide S (2010) Minimalist design of water-soluble cross-{beta} architecture. *Proc Natl Acad Sci USA* 107(8):3469–3474.
24. Wu C, et al. (2008) The binding of thioflavin T and its neutral analog BTA-1 to protofibrils of the Alzheimer's disease Abeta(16-22) peptide probed by molecular dynamics simulations. *J Mol Biol* 384(3):718–729.
25. Stsiapura VI, Maskevich AA, Kuzmitsky VA, Turoverov KK, Kuznetsova IM (2007) Computational study of thioflavin T torsional relaxation in the excited state. *J Phys Chem A* 111(22):4829–4835.
26. Maurer-Stroh S, et al. (2010) Exploring the sequence determinants of amyloid structure using position-specific scoring matrices. *Nat Methods* 7:237–242.
27. Grabowski ZR, Rotkiewicz K, Rettig W (2003) Structural changes accompanying intramolecular electron transfer: Focus on twisted intramolecular charge-transfer states and structures. *Chem Rev* 103(10):3899–4031.
28. Dzwolak W, Pecul M (2005) Chiral bias of amyloid fibrils revealed by the twisted conformation of Thioflavin T: An induced circular dichroism/DFT study. *FEBS Lett* 579(29):6601–6603.
29. Loksztejn A, Dzwolak W (2008) Chiral bifurcation in aggregating insulin: An induced circular dichroism study. *J Mol Biol* 379(1):9–16.
30. Sabate R, Lascu I, Saupe SJ (2008) On the binding of Thioflavin-T to HET-s amyloid fibrils assembled at pH 2. *J Struct Biol* 162(3):387–396.
31. Groenning M, et al. (2007) Study on the binding of Thioflavin T to beta-sheet-rich and non-beta-sheet cavities. *J Struct Biol* 158(3):358–369.
32. Krebs MR, Bromley EH, Donald AM (2005) The binding of thioflavin-T to amyloid fibrils: Localisation and implications. *J Struct Biol* 149(1):30–37.
33. McCoy AJ (2007) Solving structures of protein complexes by molecular replacement with Phaser. *Acta Crystallogr D* 63(Pt 1):32–41.
34. Murshudov GN, Vagin AA, Dodson EJ (1997) Refinement of macromolecular structures by the maximum-likelihood method. *Acta Crystallogr D* 53(Pt 3):240–255.
35. Emsley P, Cowtan K (2004) Coot: Model-building tools for molecular graphics. *Acta Crystallogr D* 60(Pt 12 Pt 1):2126–2132.
36. Collaborative Computational Project, Number 4 (1994) The CCP4 suite: Programs for protein crystallography. *Acta Crystallogr D* 50(Pt 5):760–763.
37. Adams PD, et al. (2002) PHENIX: Building new software for automated crystallographic structure determination. *Acta Crystallogr D* 58(Pt 11):1948–1954.
38. Schmidt MW, et al. (1993) General atomic and molecular electronic-structure system. *J Comput Chem* 14(11):1347–1363.
39. Lowdin PO (1950) On the non-orthogonality problem connected with the use of atomic wave functions in the theory of molecules and crystals. *J Chem Phys* 18(3):365–375.